Journal of Applied Fluid Mechanics, Vol. 14, No. 3, pp. 963-977, 2021.
Available online at www.jafmonline.net, ISSN 1735-3572, EISSN 1735-3645.
DOI: 10.47176/jafm.14.03.32210

Effect of Active Flow Control of Endwall Synthetic Jet on the Performance of a Transonic Axial Compressor

G. Wang[1], W. Chu[1,2†], H. Zhang[1] and Z. Guo[1]

[1] *School of Power and Energy, Northweatern Polytechnical University, Xi'an, Shanxi, 710129, China*
[2] *Collaborative Innovation Center of Advanced Aero-Engine, Beijing, 100191, China*

†*Corresponding Author Email: wlchu@nwpu.edu.cn*

(Received September 15, 2020; accepted November 11, 2020)

ABSTRACT

In order to improve the performance of a high-load transonic axial compressor, this paper proposes a method of applying endwall synthetic jet to the casing for active flow control. Taking NASA Rotor35 as the research object, the aerodynamic performance of the compressor is numerically calculated by applying three sets of synthetic jets with different excitation parameters at five different axial positions of 0%Ca, 25%Ca, 50%Ca, 75%Ca and 96.15%Ca. The results show that the three parameters of excitation position, jet peak velocity and jet frequency all have an effect on the performance of the compressor. The excitation position has the greatest influence on the flow margin of the compressor, and the best position is 25%Ca. After the jet peak velocity is increased from 100m/s to 150m/s, the flow margin, total pressure ratio and efficiency of the compressor are not greatly improved, which shows that the impact of the jet peak velocity is not as good as the excitation position. After continuing to increase the excitation frequency of the synthetic jet from 600Hz to 1200Hz, although the flow margin of the compressor is slightly reduced, the total pressure ratio and efficiency are further improved. This shows that there may be a threshold for the jet frequency, and only when the jet frequency is greater than the threshold can the overall aerodynamic performance of the compressor be improved.

Keywords: Transoninc axial compressor; Aerodynamic performance improve; Synthetic jet; Endwall active flow control; Numerical simulation.

NOMENCLATURE

A	area	T	synthetic jet period
Ca	axial chord length	T^*	total temperature
Cp	static pressure coefficient	t	time step
E	energy	V	velocity
f	frequency of synthetic jet		
LE	leading edge	π_r	total pressure ratio
m	mass flow	ρ	density
p	static pressure	φ	initial phase angle
p^*	total pressure	η	isotropic efficiency
r	specific heat ratio	Φ	dissipation function
R	gas constant TE	trailing edge	

1. INTRODUCTION

High-load axial compressor is one of the core components of modern aeroengines, and its performance has a crucial impact on the working performance of the engine (Saito *et al.* 2019). In high-load compressor channel, the reverse pressure gradient is strong, the pressure difference between the suction surface and the pressure surface is large, the secondary flow movement is violent, the shock wave intensity in the transonic flow field is strong, the interference between the shock wave and the

boundary layer and the leakage vortex is serious. So, it is easier to cause the separation of the boundary layer and the corner zone, resulting in huge flow loss, a decrease in aerodynamic efficiency, and may even induce rotating stall or surge, causing the compressor to enter an unstable working state. Therefore, on the basis of in-depth study of the complex flow mechanism in the compressor, proper flow control means are used to delay or weaken the flow separation, so that the compressor can not only maintain high-load operation, but also has a wide and stable working range and a high aerodynamic efficiency, which has become one of the research hotspots of the compressor aerodynamics in recent years (Ma *et al.* 2019).

From the perspective of engineering application, compared with other positions, the end wall is more suitable for flow control of the compressor. Therefore, researchers have conducted a large number of flow control experiments and numerical studies on the end wall of the compressor. Passive end wall control methods include casing treatment (Chen *et al.* 2019), end wall profiling (Li *et al.* 2014; Li *et al.* 2016), and vortex generator (Ma *et al.* 2018), etc. Because of the lack of controllable variables related to compressor operating conditions and speed changes, passive control methods usually can only optimize the performance of the compressor under individual operating conditions, therefore, it cannot guarantee that the performance of the compressor will be improved in the full range of operating conditions. In addition, although passive control methods can expand the stability margin of the compressor, it is often accompanied by a decrease in efficiency. These shortcomings may be unacceptable for high-performance compressors. In order to achieve the performance improvement requirements of compressors under all working conditions, in recent years, active control methods have also attracted the attention of many researchers in the world. Active endwall control methods include endwall surface layer suction (Xu *et al.* 2018), and plasma excitation (Zhang *et al.* 2019), etc. However, these active control methods all require complicated external pipelines and equipment. Therefore, it is currently difficult to apply to the real compressor environment.

Synthetic jet is a zero-mass jet based on vortex motion (Smith and Glezer 1998). Different from other active control methods, it has the advantages of not requiring complex piping system, compact structure, low power consumption and light weight. Therefore, it has first been systematically studied in the field of outflow, such as wings (Amitay and Glezer 2002). With the rapid development of MEMS technology, synthetic jet have also attracted more and more attention from researchers in compressor flow control. Matejka *et al.* (2008) arranged the synthetic jet exciter at the frontal position of the leading edge of a low speed compressor cascade, and conducted an experimental study on its suppression of corner separation, who found that the total outlet pressure loss and secondary flow loss were reduced by about 1.8%, 6.0%. Zander *et al.* (2011) conducted an experimental study on the secondary flow in the endwall of a compressor cascade controlled by synthetic jet, and the results showed that when the exciter is located upstream of the separation point and the jet angle is small, the flow control effect is better. De Giorgi *et al.* (2012) believes that the synthetic jet enhances the generation of vortices in the jet exit flow field, promotes the momentum mixing between the low energy fluid in the boundary layer and the main flow, so that the separated boundary layer can overcome the reverse pressure gradient and maintain reattachment. Culley *et al.* (2004) arranged 6 synthetic jet excitation holes on the suction surface of the compressor stator blade. Experimental results showed that the synthetic jet delayed the flow separation at the hub and reduced the total pressure loss by 4%. Zheng *et al.* (2006) verified the effectiveness of arranging synthetic jets on the suction surface of the blade and the casing respectively for flow separation control on a compressor cascade test bench. Using a high-speed compressor cascade as numerical simulation object, Qin *et al.* (2017) took a low speed and high speed compressor cascades as numerical simulation objects, carried out a parametric study on the synthetic jet of suction surface and endwall, and revealed the mechanism of the synthetic jet to control the corner separation of the cascade and reduce the loss.

It can be found that many existing studies conducted in the compressor cascade show that the synthetic jet can reduce the flow loss, but the application research of this flow control technology in real compressor environment is still extremely rare. The groundbreaking research work came from Benini *et al.* (2011), who arranged the synthetic jet on the suction surface of the transonic compressor NASA Rotor37. The results of numerical simulation showed that compared with the prototype, the aerodynamic efficiency of the rotor excited by synthetic jet near the stall point was increased by 1.4 %. Although the existing synthetic jet excitation cannot reach the jet peak velocity in the Benini's simulation, it fully shows that this flow control technology has the application potential in real compressor. In fact, although the effect of applying synthetic jet excitation on the compressor rotor blades may be better, the thickness of the rotor blades is very thin and the rotation speed is high, which may be difficult to use in engineering. Therefore, this paper proposes to apply synthetic jet excitation on the casing of a transonic axial flow compressor. It is understood that there is no public literature report on this research.

2. RESEARCH OBJECTS AND METHODS

2.1 Numerical Model and Validation

Take the typical transonic axial flow compressor NASA Rotor35 as the research object. It is the rotor part of Stage35, which is an inlet stage of a transonic axial compressor designed by Reid and Moore (1978). Although it was designed in the 1970s, it has the typical characteristics of modern

transonic axial flow compressor. Many researchers take it as the object of studying the flow field of transonic axial flow compressors and testing the effect of flow control (Biela *al.* 2008; Yamada *al.* 2008). Rotor35 has 36 blades, aspect ratio 1.19, hub ratio 0.7, design flow rate is 20.188kg/s, design total pressure ratio and adiabatic efficiency are 1.865 and 0.865 respectively, design speed is 17188.7rpm, and tip speed is 454.456m/ s. More design parameters can refer to literature (Reid and Moore 1978).

The grid for numerical calculation is generated by IGG/Autogrid5. 93 nodes are arranged in the radial direction. The O4H grid topology is adopted around the blade, in which 217 nodes are arranged around the blade. The blade tip clearance adopts a butterfly-shaped grid topology structure with 17 nodes arranged along the radial direction. The inlet and outlet of the compressor adopt H-shaped grid. The grids near the wall are all encrypted, and the distance of the first layer of grids is 3μm, ensuring $y+<1$. The computational grid nodes of the prototype compressor are approximately 1.8 million. As shown in Fig. 1.

The commercial software, ANSYS CFX 18.0, is utilized to perform single channel numerical calculations at 100% design speed. The fluid is set to ideal gas, *κ-ω SST* is selected as the turbulence model (Benini *et al.* 2011), the convection term and turbulence term are in high precision format, the inlet boundary conditions are set to an absolute total pressure of 101325Pa, an absolute total temperature of 288.15K, and an inlet air turbulence degree to 5%, the outlet boundary condition is set to average static pressure.

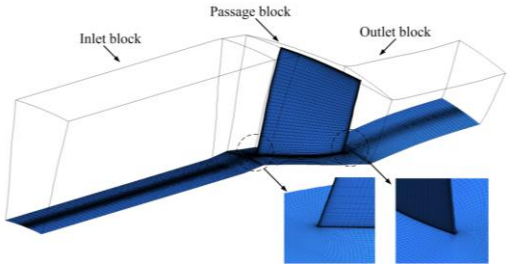

Fig. 1. Computational grid.

Figure 2 shows the comparison between experimental measurement values and numerical calculation values. Compared with the experimental results, the numerically calculated blockage point flow rate is lower, the total pressure ratio is also lower, but the efficiency is in good agreement. The reason for these errors may be related to factors such as turbulence model and ideal gas assumption. Figure 3 shows the tangential velocity distribution of three different cross-sections between the experimental measurement (Van Zante 2000) and the numerical calculation at the peak efficiency point. It can be seen from the figure that both the numerical value and the distribution of the leakage vortex, the results of numerical calculation and experimental measurement are in good agreement. Therefore, it can be considered that the numerical model established in this paper is reliable.

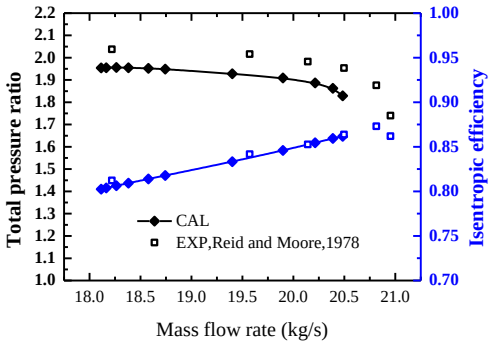

Fig. 2. Total performance of compressor between experiment and simulation.

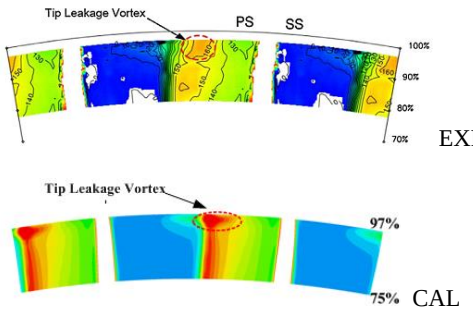

(a) 33% of Ca

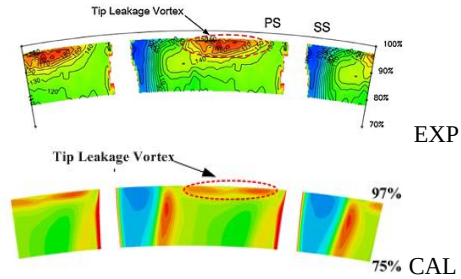

(b) 55% of Ca

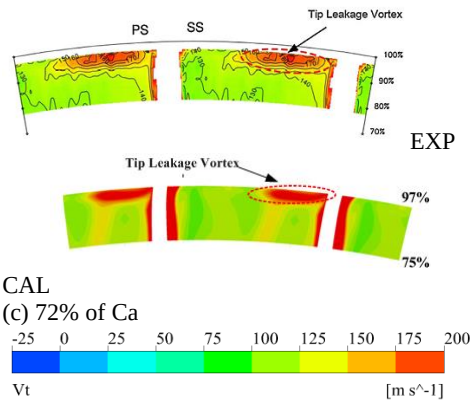

(c) 72% of Ca

Fig. 3. Experimental measured and numerical calculated tangential velocity distribution on cross-sections at PE.

2.2 Flow Control Method

In order to simulate the synthetic jet on the endwall of the compressor, a circumferential groove with width and depth of 1mm is designed on the casing. The position of the groove is described by the distance L between the front wall of the groove and the leading edge of the blade tip, as shown in Fig. 4. The groove wall is set as the adiabatic non-slip wall condition, and the groove top is set as the speed inlet condition. The speed expression is listed as follows:

$$V(t) = V_{\max} \sin(2\pi ft + \varphi) \tag{1}$$

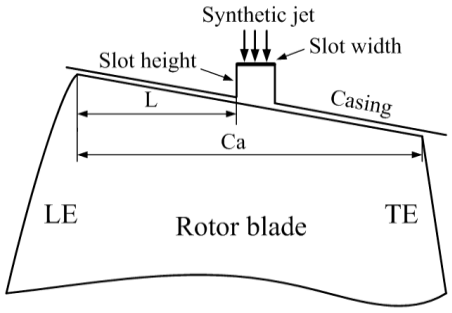

Fig. 4. Geometric construction of synthetic jet.

Since the circumferential coverage of the synthetic jet is 100%, the initial phase angle has no effect on the result, so the initial jet angle is set to 0 in this paper.

The endwall synthetic jet includes three key parameters: axial position, jet peak velocity, and jet frequency. In this paper, a total of 5 axial positions were studied, namely 0%Ca, 25%Ca, 50%Ca, 75%Ca and 96.15%Ca. According to Benini's approach, the reference jet frequency of the synthetic jet is set to 600Hz, and the jet peak velocity is set to 100m/s. Then, according to the response of the flow field, the jet peak velocity and frequency are respectively increased and then calculated. In this paper, three sets of parameters are calculated at the above five positions, a total of 15 schemes: V_{max}=100m/s, f=600Hz; V_{max}=150m/s, f=600Hz; V_{max}=150m/s, f=1200Hz. In transient simulation, the discretization of the time term adopts the second-order backward Euler format, the time step is set to 1/20 of the injection/suction cycle of a synthetic jet, and the maximum number of iterations in each time step is 10.

3. RESULT ANALYSIS

3.1 Stall Mechanism of Transonic Compressor Rotor35

It can be seen from Fig. 5(a) that when the prototype compressor is at the design point, the airflow in the blade tip channel flows smoothly, There is a clear positive shock wave at the entrance of the blade, and the trailing edge of the suction surface is slightly separated. It can be seen from Fig. 6(a) that the tip leakage flow is divided into three sections at the design point. The leakage flow at the leading edge and the middle of the tip passes through the shock wave, and the speed decreases, and they enclose each other out of the compressor channel. Leakage from the trailing edge of the blade flows directly out of the compressor channel. As shown in Fig. 5(b), as the back pressure increases to near stall conditions, The positive shock wave moves forward to form an off-body shock wave, and the separation range of the suction surface is also significantly increased, forming the first low speed zone in the channel. At the same time, the second low speed zone with a larger area and lower speed appears in the center of the channel. It can be seen from Fig. 6(b) that this is due to the fact that the leakage flow of tip leading edge interacts with the channel main flow after passing through the shock wave under the adverse pressure gradient, forming a tip leakage vortex with obvious curling phenomenon, which blocks the tip channel. Only a small part of the leakage flow in the middle and rear of the blade can flow out of the compressor channel under the action of the reverse pressure gradient, and most of it is engulfed in the tip leakage vortex to form a secondary leakage. Therefore, the two low speed zones formed by the separation of the tip leakage vortex and the suction surface flow almost block the entire channel, causing a sharp drop in the flow capacity, which is the main cause of the compressor stall.

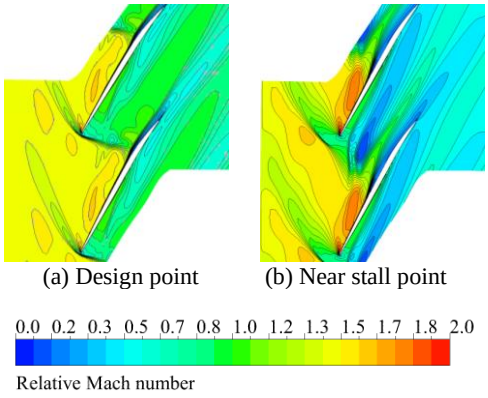

Fig. 5. Relative Mach number of 95% span.

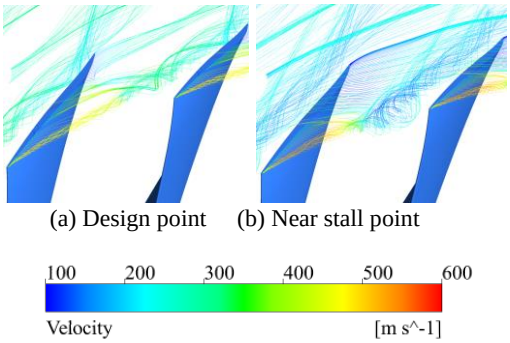

Fig. 6. Distribution of tip leakage flow streamline.

3.2 The Effect of Synthetic Jet on the Overall Performance of Transonic Compressor

The synthetic jet input energy to the compressor, and the influence of this part of energy should be considered when calculating the compressor efficiency. Fortunately, Bae *et al.* (2005) proposed a synthetic jet energy calculation method:

$$E = 0.5\rho A(0.26V_{\max}^3) \tag{2}$$

Therefore, the compressor efficiency calculation formula considering the energy input of the synthetic jet is modified as follows:

$$\eta = ((p_2^* / p_1^*)^{\wedge}((\gamma-1)/\gamma)-1)\Big/(T_2^*/T_1^*-1 + E/m/(\gamma/(\gamma-1))/R/T_1^*) \tag{3}$$

In order to compare the total performance of the prototype compressor and the compressor after the synthetic jet is applied, three parameters are introduced: flow margin change ΔSM, total pressure ratio change $\Delta\pi_r$, and efficiency change $\Delta\eta$:

$$\Delta SM = \left[(m_{baseline} - m_{sj})/m_{baseline}\right]\times 100\% \tag{4}$$

$$\Delta\pi_r = (\pi_{r.sj}/\pi_{r.baseline} - 1)\times 100\% \tag{5}$$

$$\Delta\eta = (\eta_{sj}/\eta_{baseline} - 1)\times 100\% \tag{6}$$

Figure 7 shows the overall performance diagram of the compressor under the excitation of synthetic jet. It can be seen from the figure that although the effects of synthetic jets with different parameters are not the same, the general rules of their effects on compressor performance can be obtained from it.

It can be seen from Fig. 8 that no matter what jet parameter is excited, the change of the compressor flow margin shows a law of first increasing and then decreasing compared to the prototype compressor. The flow margin under excitation of 0%Ca and 96.15%Ca decreases. The flow margin under 25%Ca excitation is significantly expanded. The flow margin under the excitation of the other two positions does not change much. Therefore, 25%Ca is the best position for the endwall synthetic jet. Under the excitation of the three sets of different parameters at this position, the flow margin of the compressor is expanded by 6.07%, 7.22%, and 5.65% respectively.

It can be seen from Fig. 9(a) that at the design point, the change in total pressure ratio of the compressor shows a law of first increasing and then decreasing. When jet peak velocity is 100m/s, compared with the prototype compressor, the total pressure ratio under 0%Ca excitation is reduced, the total pressure ratio under 96.15%Ca excitation is almost unchanged, while the total pressure ratio under excitation at the other three positions are increased, and the maximum total pressure ratio is obtained when excited by 50%Ca. At the same time, from the perspective of the influence of excitation parameters, the change in the total pressure ratio of the compressor increases with the increase of jet peak velocity, and also with the increase of jet frequency. This indicates that at the design point, jet position, jet peak velocity and jet frequency all have an effect on the total pressure ratio of the compressor. At the near stall point of the prototype compressor, it can be seen from Fig. 9(b) that jet peak velocity increases from 100m/s to 150m/s. Although the total pressure ratio of the compressor has increased, it is still lower than the prototype compressor. However, jet frequency was increased from 600 Hz to 1200 Hz, and the total pressure ratio of the compressor was greatly increased and was higher than that of the prototype compressor. This indicates that at the near stall point, jet frequency has a greater impact on the total compressor pressure ratio than jet peak velocity.

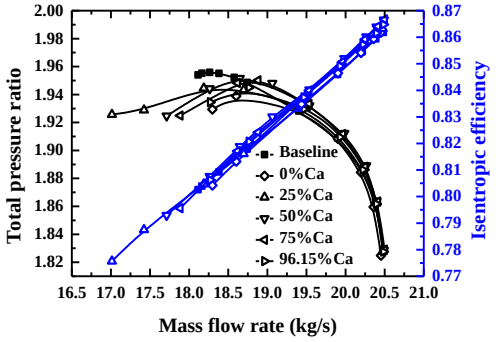

(a) Vmax=100m/s, f=600Hz

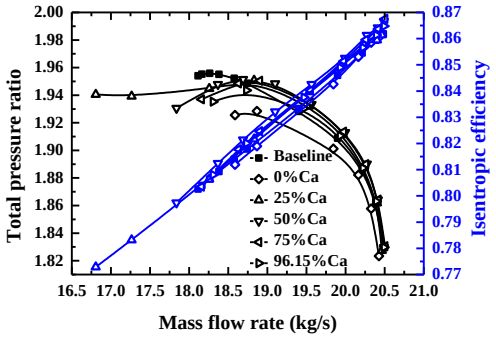

(b) Vmax=150m/s, f=600Hz

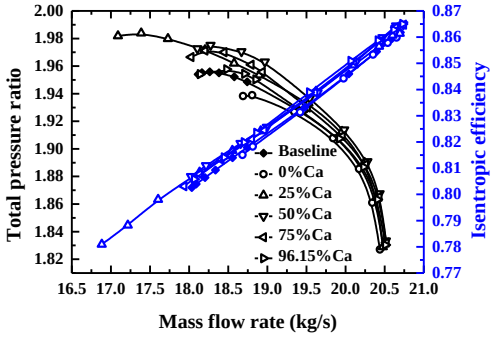

(c) Vmax =150m/s, f=1200Hz

Fig. 7. Total performance of compressor under endwall synthetic jet with different excitation parameters.

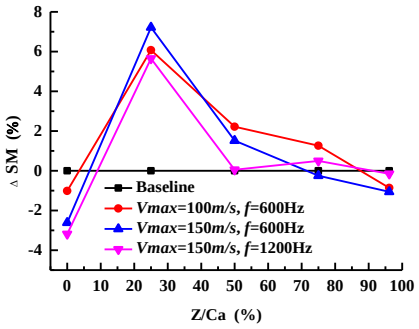

Fig. 8. ΔSM **as a function with excitation position.**

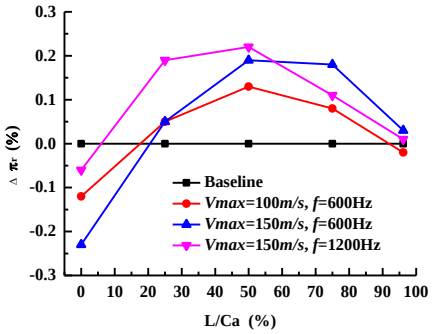

(a) design point

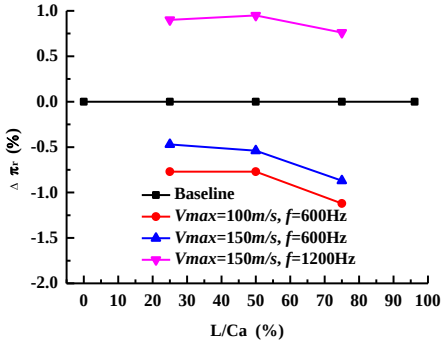

(b) near stall point

Fig. 9. $\Delta\pi_r$ **as a function with excitation position.**

It can be seen from Fig. 10(a) that at the design point, the change in efficiency of the compressor also shows a law of first increasing and then decreasing. When jet peak velocity is 100m/s, compared with the prototype compressor, the efficiency under 0%Ca excitation is reduced, and the efficiency under excitation at other four positions is increased, and when the synthetic jet is excited by 50% Ca, the efficiency is increased the most, reaching 0.8%. At the near stall point of the prototype compressor, it can be seen from Fig. 10(b) that when jet peak velocity increases from 100m/s to 150m/s, the efficiency of the compressor increases. When jet frequency is increased from 600Hz to 1200Hz, the efficiency of the compressor continues to increase, and the efficiency under 25%Ca and 50%Ca excitation increases by 0.49% and 0.5% respectively. This indicates that near the stall point, jet frequency and jet peak velocity both have an impact on the compressor efficiency.

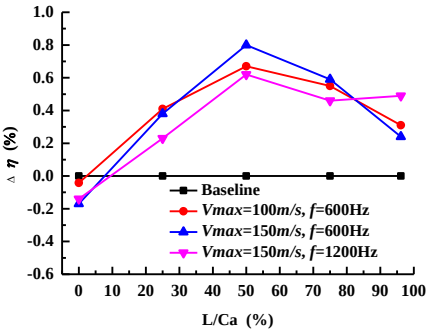

(a) design point

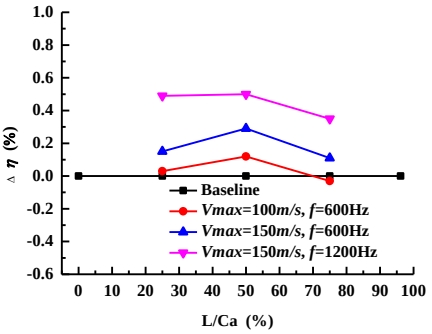

(b) near stall point

Fig. 10. $\Delta\eta$ **as a function with excitation position.**

3.3 Internal Flow Field Analysis

In order to reveal the mechanism of the compressor flow margin change when the synthetic jet is at different positions, three typical positions of 0%Ca, 25%Ca and 50%Ca are taken as examples for analysis. Figure 11 shows the relative Mach number contour map at 95%span. Where, the compressor under 0%Ca excitation is in near stall condition, and the compressor flow under 25%Ca and 50%Ca excitation is approximately equal to the prototype compressor near stall condition.

It can be seen from Fig. 11(a) that after the synthetic jet is applied with 0% Ca (0T means the synthetic jet is at the initial moment of the injection phase, 0.25T is at the maximum injection moment, 0.5T is at the initial moment of the suction phase, 0.75T is at the maximum suction moment, the same below), because the excitation position is before the second low speed zone of the prototype compressor, and it crosses the shock wave, when the synthetic jet is in the injection phase, as the jet velocity increases, the jet airflow is blocked by the shock wave, and is entrapped by the tip leakage flow from the leading edge of the blade tip, causing the leakage flow to increase, and the velocity decreases

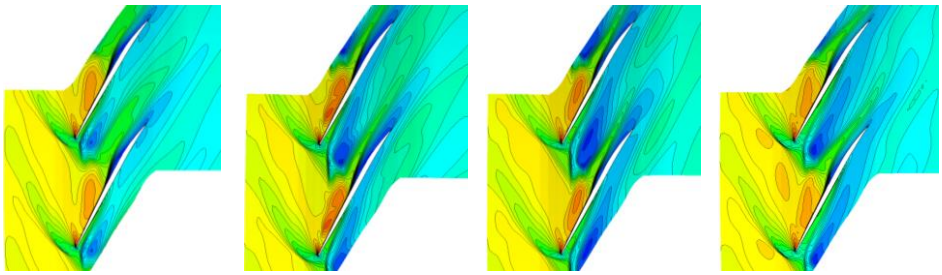

(1) 0T (2) 0.25T (3) 0.5T (4) 0.75T

(a) 0%Ca synthetic jet excitation (Vmax=150m/s, f=1200Hz)

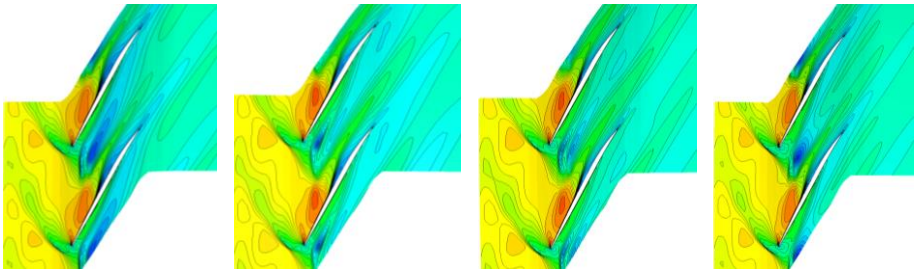

(1) 0T (2) 0.25T (3) 0.5T (4) 0.75T

(b) 25%Ca synthetic jet excitation (Vmax=100m/s, f=600Hz)

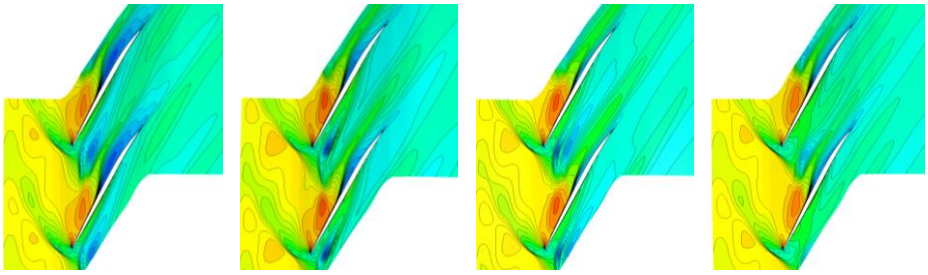

(1) 0T (2) 0.25T (3) 0.5T (4) 0.75T

(c) 25%Ca synthetic jet excitation (Vmax=150m/s, f=600Hz)

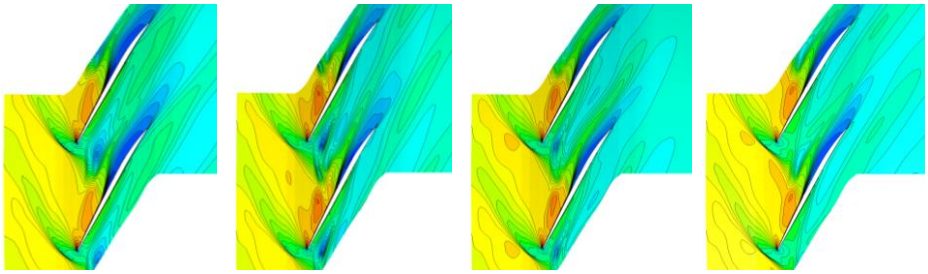

(1) 0T (2) 0.25T (3) 0.5T (4) 0.75T

(d) 25%Ca synthetic jet excitation (Vmax=150m/s, f=1200Hz)

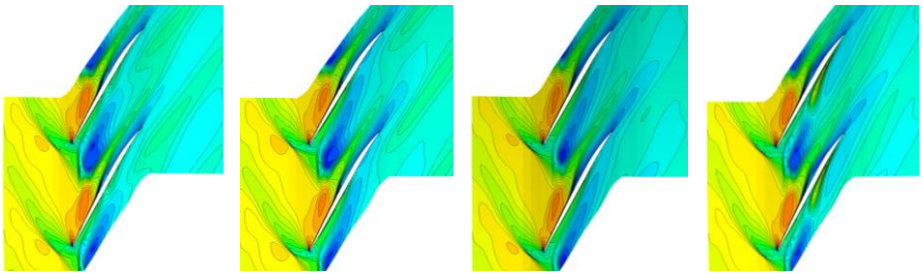

(1) 0T (2) 0.25T (3) 0.5T (4) 0.75T

(e) 50%Ca synthetic jet excitation (Vmax=150m/s, f=1200Hz)

Fig. 11. Relative Mach number of 95% span.

after crossing the shock wave and converges at the tip of the blade, the strength of the tip leakage vortex is also increasing, resulting in an increase in the area of the second low speed zone after the shock wave. At this time, the compressor is more clogged than the prototype compressor. At 0.5T, the area of low speed zone reaches the maximum, and the rotor is in the most severely blocked state. Then the synthetic jet enters the suction phase, and the area of the second low speed zone is reduced. By the time of 0T in the next cycle, the blockage area reaches the minimum, and the degree of blockage is equivalent to that of the prototype compressor. This indicates that for this position, the suction effect of synthetic jet is more effective than the injection effect. However, on the whole, when the synthetic jet is at the 0%Ca position, the compressor blockage is more serious than the prototype during a synthetic jet cycle, so the flow margin is correspondingly lower than that of the prototype compressor.

It can be seen from Fig. 11(b) that after the synthetic jet is applied at the position of 25% Ca, the jet velocity of the synthetic jet is 0 at 0T. At this time, the degree of clogging of the compressor blade tip is equivalent to that of the prototype compressor. With the increase of the injection velocity of synthetic jet, since the position of the synthetic jet is exactly in the second low speed zone, the low speed airflow at the tip of the blade is blown downstream under the action of the jet airflow, the range of the tip leakage vortex and the intensity are both reduced, and the blockage of the compressor tip is getting smaller and smaller. At 0.25T, jet peak velocity reaches the maximum, the original second low velocity zone is divided into two parts, the blockage range is minimized, and the degree of separation of the trailing edge of the suction surface is also reduced. Then, as the injection velocity of the synthetic jet decreases, the blockage range of the second low velocity zone slightly increases. At 0.5T, the synthetic jet enters to the suction phase. As the suction speed becomes larger and larger, the blade tip clogging range begins to increase. The second low speed zone divided into two regions is merged into one again, but the degree of clogging is still smaller than the prototype compressor. Therefore, when the synthetic jet is at the position of 25%Ca, its injection effect is more beneficial than the suction effect for enlarging the compressor margin.

Comparing Fig. 11(b) and (c), on the basis of keeping the jet frequency at 600Hz, the jet peak velocity increases from 100m/s to 150m/s. During the injection phase, the effect of synthetic jet on the tip blockage was not significant. However, in the suction phase, the suction effect of the synthetic jet on the low speed airflow at the tip of the blade makes the compressor tip clogging range smaller. At the maximum suction moment of 0.75T, the tip clogging is almost completely eliminated. Therefore, after the jet peak velocity increases, the flow margin of the compressor is also greater.

Comparing Fig. 11(c) and (d), on the basis of maintaining the jet peak velocity of 150m/s, the jet frequency is increased from 600Hz to 1200Hz. Comparing the blockage of the tip channel at the corresponding time, it is found that the tip leakage vortex is weaker and the blocking range is also smaller, which is the result of increased jet frequency. However, it is precisely because of the increase in jet frequency that the separation of trailing edge of the suction surface is more greater. At the same time, the degree of compressor blockage is also increased. Therefore, after the jet frequency increases, the flow margin of the compressor decreases.

It can be seen from Fig. 11(e) that after the synthetic jet is applied with 50%Ca, when the synthetic jet is in the injection phase, the separation of boundary layer at the trailing edge of the suction surface does not change much, but because the excitation position is downstream of the second low speed region, the injection effect of the synthetic jet strengthens the spread of the tip leakage vortex to the downstream of the channel, resulting in an increase in the tip leakage vortex's intensity and scope, and further enlarges the area of the second low speed region, causes compressor blockage to become more serious. When synthetic jet is in the suction phase, the suction effect of the synthetic jet prevents the tip leakage vortex from spreading downstream, and also increases the air velocity in the rear section of the blade near the pressure surface. However, because the suction position is downstream of the blocked core area, although the blockage range is smaller than the injection phase, the degree of blockage is still greater than that of the prototype compressor, and it is impossible to change the compressor near the stall state.

In order to further explore the mechanism of the change of the total pressure ratio of the compressor under the excitation of different synthetic jet parameters, Figure 12 shows the distribution of the static pressure coefficient of the compressor at 95%span. The flow conditions of the prototype compressor and the compressor with synthetic jet excitation are the same as those in Fig. 11. The static pressure coefficient *Cp* is defined as follows:

$$Cp = (p - p_{in}) / (p_{in}^{*} - p_{in}) \tag{7}$$

It can be seen from Fig. 12(a) that after the synthetic jet is applied with 0% Ca, the static pressure coefficient of the pressure surface is lower than the prototype compressor during the entire jet cycle. Looking at the suction surface, although the static pressure coefficient is greater than the prototype before 30%Ca, the local flow near this position of the compressor is also improved, and the shock wave moves from about 30%Ca to about 40%Ca, but from 30%Ca to the trailing edge of the blade, the static pressure coefficient is greatly reduced compared to the prototype compressor, and the decrease of the static pressure coefficient

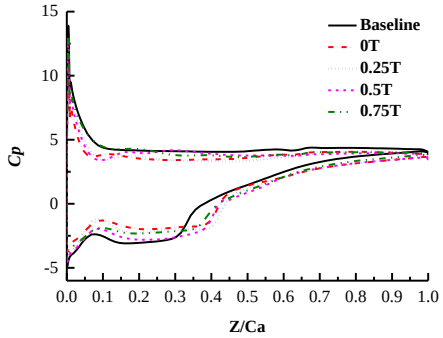

(a) 0%Ca synthetic jet excitation (V_{max}=150m/s, f=1200Hz)

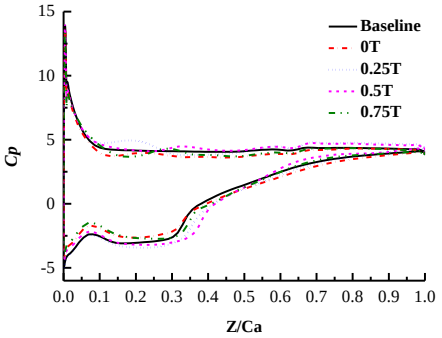

(c) 25%Ca synthetic jet excitation (V_{max} =150m/s, f=600Hz)

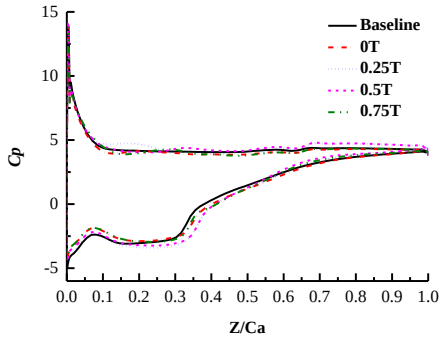

(b) 25%Ca synthetic jet excitation (V_{max}=100m/s, f=600Hz)

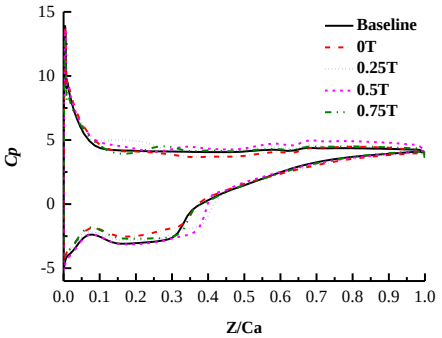

(d) 25%Ca synthetic jet excitation (V_{max} =150m/s, f=1200Hz)

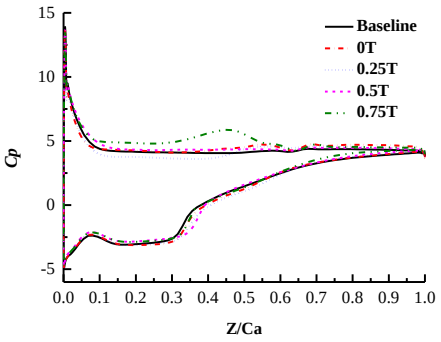

(e) 50%Ca synthetic jet excitation (V_{max} =150m/s, f=1200Hz)

Fig. 12. Static pressure distribution of 95% span.

indicates that the separation of the suction surface is increased. Synthesizing the changes in the static pressure coefficient of the pressure surface and the suction surface, it can be inferred that compared with the prototype compressor, the compressor load after the synthetic jet is applied with 0% Ca is reduced, so the total pressure ratio is also reduced accordingly.

It can be seen from Fig. 12(b) that after the synthetic jet is applied at 25%Ca, the static pressure coefficient on the pressure side does not change much, and the suction side increases slightly before 20%Ca, while the static pressure coefficient between 20%Ca and 50%Ca decreases significantly, therefore, the compressor load is reduced, and the total pressure ratio relative to the prototype is also reduced accordingly. When the jet peak velocity increases from 100m/s to 150m/s, it can be seen from Fig. 12(c) that the fluctuation of the static pressure coefficient on the pressure surface side increases, but the average value is still lower than the prototype. Looking at the suction surface, the static pressure coefficient before 20%Ca increases, and it decreases even more between 20%Ca and 50%Ca. Therefore, at this time, the total pressure ratio of the compressor is

greater than the jet peak velocity of 100m/s, but still lower than the prototype. When the synthetic jet frequency is increased from 600Hz to 1200Hz, it can be seen from Fig. 12(d) that compared with the prototype compressor, the static pressure coefficient of the pressure surface increases throughout the injection phase. The static pressure coefficient of the suction surface before about 32%Ca is also greater than that of the prototype. The shock wave moves from about 30%Ca to about 40%Ca in the injection phase, and is equivalent to the prototype in the suction phase, indicating the compressor's flow capacity enhanced. The static pressure coefficient of the suction surface after 45%Ca is almost unchanged, indicating that the separation of the surface layer has almost no change. On the whole, the compressor load increases, so the total pressure ratio increases.

It can be seen from Fig. 12(e) that after the synthetic jet is applied with 50% Ca, the static pressure coefficient of the suction surface decreases slightly during the injection phase, and the shock wave position moves back slightly. The static pressure coefficient of the pressure surface fluctuates significantly. During the injection phase, the static pressure coefficient of the pressure surface decreases first and then rises. During the suction phase, the static pressure coefficient of the pressure surface continues to increase. The increase in static pressure indicates that the compressor load increases and the total pressure ratio increases accordingly.

Entropy is a direct reflection of loss, and high entropy area corresponds to high loss area. In order to explore the mechanism of compressor efficiency change, Fig. 13 shows the entropy distribution map of five equidistant sections on the blade under design point conditions. It can be seen from Fig. 13(b) that after the synthetic jet is applied at 0%Ca, during the injection phase, as mentioned above, because the excitation position is before the shock wave, the injection of jet airflow causes more serious blockage of the compressor blade. Therefore, the entropy increases correspondingly, and the loss also increases. In the suction phase, the situation is the opposite. The synthetic jet sucks away part of the leakage flow at the leading edge of the blade tip, weakens the strength of the leakage vortex, and reduces the leakage flow rate. Therefore, the entropy is reduced.

After applying the synthetic jet with 25%Ca, it can be seen from Fig. 13(c) that the effect of applying the synthetic jet with 0%Ca is different. Since the excitation position is just above the tip blockage at this time, during the injection phase, the jet effect of synthetic jet will blow away the low speed air flow at the blade tip, reducing the high entropy zone. In the suction phase, the suction effect of synthetic jet sucks out the low speed airflow at the tip of the blade, and the high entropy zone is further reduced. The reduction of the loss means the improvement of the compressor efficiency. At the same time, it can be seen that the suction effect of the synthetic jet is more advantageous than the ejection effect in reducing losses.

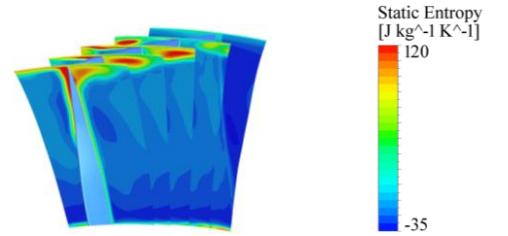

(a) Baseline

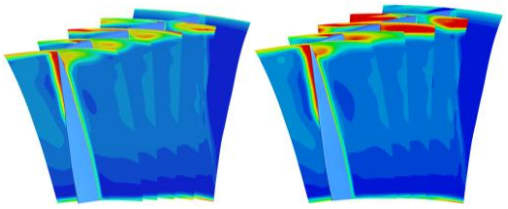

(1) 0T (2) 0.25T

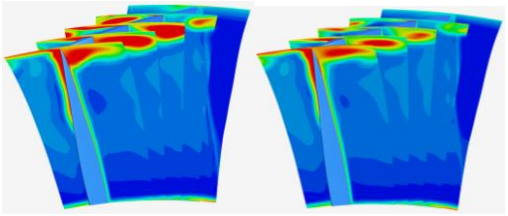

(3) 0.5T (4) 0.75T

(b) 0%Ca synthetic jet excitation (Vmax=150m/s，f=1200Hz)

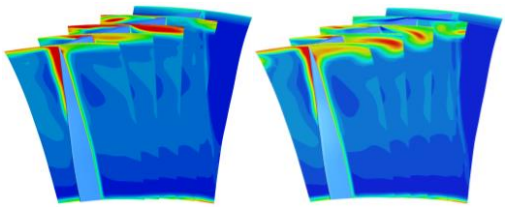

(1) 0T (2) 0.25T

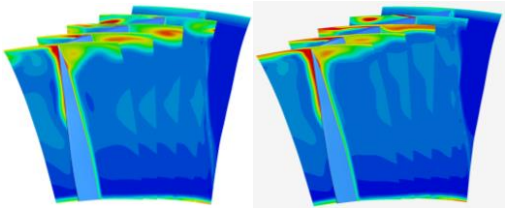

(3) 0.5T (4) 0.75T

(c) 25%Ca synthetic jet excitation (Vmax=150m/s，f=1200Hz).

Fig. 13. Distribution of static entropy at design point.

Figure 14 shows the entropy distribution of five equidistant sections on the blade when the prototype compressor is at the near the stall point. It can be seen from Fig. 14(a) that under near stall conditions, because the tip leakage flow of the prototype compressor gathers more at the tip, the separation range of the trailing edge of the suction surface is further expanded, and the compressor blockage is more serious. Therefore, The range of

high entropy zone is also larger than that at the design point.

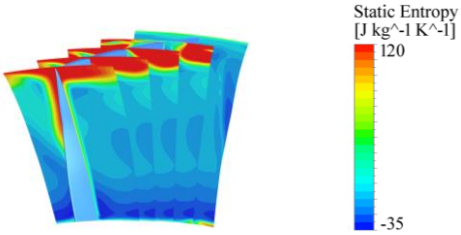

(a) Baseline

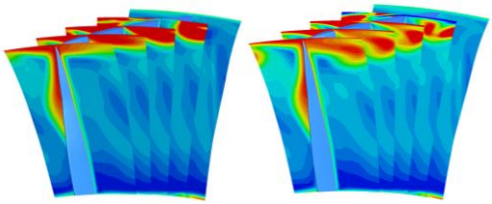

(1) 0T (2) 0.25T

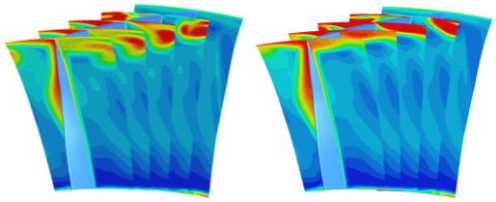

(3) 0.5T (4) 0.75T

(b) 25%Ca synthetic jet excitation (Vmax=100m/s，f=600Hz)

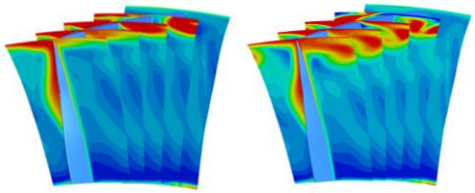

(1) 0T (2) 0.25T

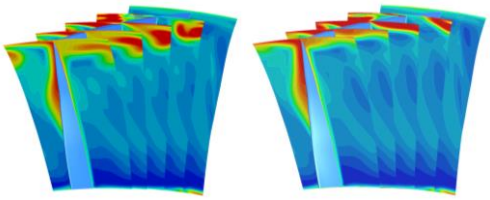

(3) 0.5T (4) 0.75T

(c) 25%Ca synthetic jet excitation (Vmax=150m/s，f=600Hz)

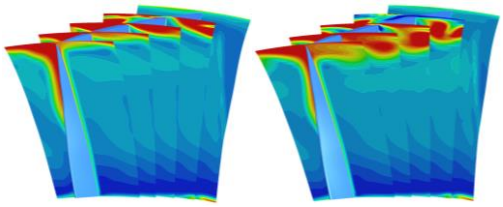

(1) 0T (2) 0.25T

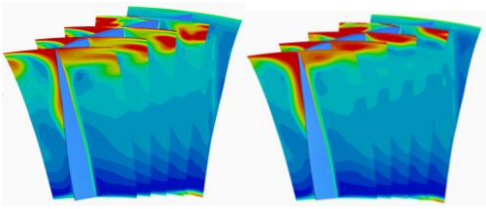

(3) 0.5T (4) 0.75T

(d) 25%Ca synthetic jet excitation (Vmax=150m/s，f=1200Hz)

Fig. 14. Distribution of static entropy at near stall point.

After applying the synthetic jet at 25%Ca, it can be seen from Fig. 14(b) that when the jet peak velocity is 100m/s, the tip leakage flow is blown away by the jet during the injecton phase. The leakage flow rate decreases, the strength of the tip leakage vortex gradually decreases, and the range of the high entropy zone decreases. In the suction phase, as the suction speed increases (0.75T), the range of high entropy zone is further reduced, but as the suction speed decreases (0T), the range and intensity of high entropy zone increase rapidly. After the jet peak velocity is increased to 150m/s, it can be seen from Fig. 14(c) that the range of high entropy zone does not change much during the injection phase, but the range of high entropy zone is smaller during the suction phase, so the loss is smaller too. When the jet frequency increases to 1200Hz, the entropy in the channel further decreases, but the entropy increases slightly due to the increased separation of the trailing edge of the suction surface.

There are many sources of loss in the compressor channel, and the loss in different positions corresponds to different mechanisms. Li explored the causes of loss from the perspective of fluid dissipation. By introducing the concept of loss source, he proposed a definition to describe the three-dimensional loss in the compressor cascade (Li *et al.* 2014; Li *et al.* 2016). The loss caused by different sources can be obtained by integrating the volume of the dissipation function in the corresponding region, and then using the inlet dynamic pressure dimensionless to obtain the loss source, which is defined as follows:

$$\gamma_{source}=\frac{\Delta p^{*}_{source}}{p^{*}_{in}-p_{in}}=\frac{\iiint_{region}\Phi \mathrm{d}x\mathrm{d}y\mathrm{d}z}{(p^{*}-p)_{in}\iint_{in}V_n\mathrm{d}A} \tag{8}$$

Where γ_{source} is the loss source, Δp^{*}_{source} is the total pressure loss caused by a specific source, the subscript *in* represents the inlet measurement section, and V_n and A are the normal velocity and the area of integral surface respectively.
Φ represents the dissipation function, and its tensor form is defined as follows:

$$\Phi(x,y,z)=\frac{\mu_{eff}}{2}\left(\frac{\partial u_i}{\partial x_j}+\frac{\partial u_j}{\partial x_i}\right)^2-\frac{2}{3}\mu_{eff}\left(\frac{\partial u_i}{\partial x_i}\right)^2 \tag{9}$$

Where u represents speed, μ_{eff} represents the comprehensive viscosity coefficient, which is equal

to the sum of the dynamic viscosity of the fluid and the turbulent viscosity.

With reference to Li's method of classifying losses, this paper further extends it to the description of losses in the transonic compressor rotor. As shown in Fig. 15, the loss source and the corresponding dissipation function integral area are divided into 6 parts:

(1) Inlet section loss: γ_{IN}. The axial range is the area from the inlet measurement interface to the leading edge of blade root, and the radial range is from the hub to casing, and the area $\log_{10}(\nabla p) < 7$.

(2) Outlet section loss: γ_{OUT}. The axial range is from the trailing edge of blade root to the outlet measurement interface, and the radial range is the area from the hub to casing.

(3) Hub endwall loss: γ_{HUB}. The axial range is from the leading edge to the trailing edge of blade root, and the radial range is the area from hub to 2% span. It is worth noting that 2% span is not the boundary thickness, but approximates the scale of strong shear flow near the wall due to hub friction.

(4) Shock loss : γ_{SHK}. Divided into two parts: ①The axial range is from the leading edge to the trailing edge of blade root, and the radial range is from 85%span to casing, and the area $\log_{10}(\nabla p) \geq 7$; ②Inlet measurement surface to the leading edge of blade root, the radial range is the area between hub and casing, and the area $\log_{10}(\nabla p) \geq 7$. It is worth noting that shock loss zone comes from the observation of flow field. Since it is found that pressure gradient near the shock wave is generally greater than 10^7Pa/m, the area where $\log_{10}(\nabla p) \geq 7$ is specified as the impact range of shock wave.

(5) Tip leakage and separation loss: γ_{TL}. The axial range is from the leading edge to the trailing edge of the blade root, and the radial range is from 85% span to casing, and the area $\log_{10}(\nabla p) < 7$.

(6) Passage separation loss: γ_{PAS}. Other area.

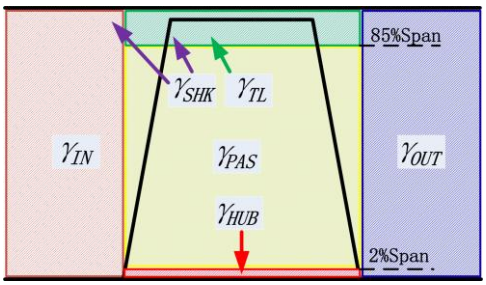

Fig. 15. Loss source division.

Figure 16 shows the changes in the loss sources of 6 areas relative to the prototype compressor when synthetic jet excitation is applied at 0%Ca and 25%Ca at design point. It can be seen from the figure that among the 6 loss sources, shock loss, blade tip leakage and separation loss vary greatly. After the excitation position of synthetic jet is moved backward from 0%Ca to 25%Ca, the shock wave loss decreases during the suction stage, also decreases at the time of maximum suction, and does not change much at the time of maximum injection, which indicates that the suction effect of 25%Ca synthetic jet can weaken the intensity of shock wave more than 0%Ca. In addition to the initial time of injection 0T, the tip leakage and separation loss is also reduced, which indicates that when synthetic jet is at 25% Ca, the suppression of tip leakage and tip separation is more effective than at 0% Ca. The reduction of loss in the outlet section indicates that when the synthetic jet is at 25% Ca, the air mixing at the outlet section of the compressor is more uniform and the loss is smaller.

Figure 17 shows the changes in the loss sources of 6 areas relative to the prototype compressor when synthetic jets with different excitation parameters are applied to 25%Ca at near stall point. It can be seen from the figure that the biggest impact on compressor loss is still shock loss, blade tip leakage and separation loss. After the jet peak velocity is increased from 100m/s to 150m/s, the tip leakage, separation loss and channel separation loss are reduced, which indicate that after the jet peak velocity is increased, the injection and suction is more effective on the tip leakage flow, the separation of suction surface is smaller, but the shock loss increases at the time of maximum injection and maximum suction. After the jet frequency is increased from 600 Hz to 1200Hz, the loss in the outlet section is reduced, which indicates that the compressor is more uniformly mixed. Shock loss, tip leakage and separation loss decrease in the injection phase, but increase in the suction phase, indicating that increasing the jet frequency in the injection phase can weaken the intensity of the shock, reduce the tip leakage and the separation of the suction surface. However, the excessively high frequency seems to increase the loss during the suction phase.

4. CONCLUSION

A method for active flow control of a transonic axial compressor using synthetic jet on the endwall is proposed. Through numerical simulation of synthetic jet with 5 positions and 3 sets of parameters, the following conclusions are obtained:

(1) Under near stall condition, the tip leakage flow of the prototype compressor can not flow smoothly out of the compressor passage under the action of the reverse pressure gradient after passing through the shock wave. Instead, it accumulates in the tip passage and forms the tip leakage vortex, the vortex core expands with the increase of the reverse pressure, which leads to the blockage of the blade tip. At the same time, the suction surface layer is also severely

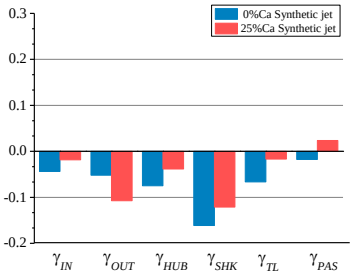

(a) 0T

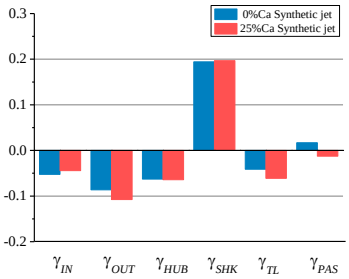

(b) 0.25T

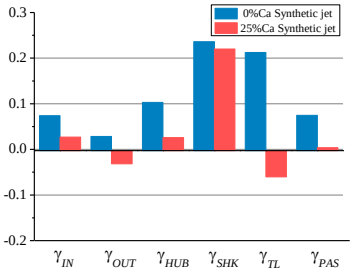

(c) 0.5T

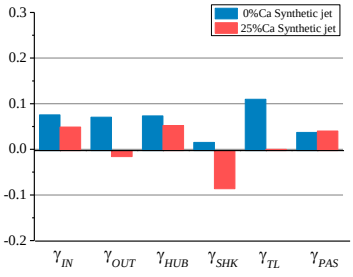

(d) 0.75T

Fig. 16. Loss source change under synthetic jet excitation at design point (Vmax=150m/s, f=1200Hz).

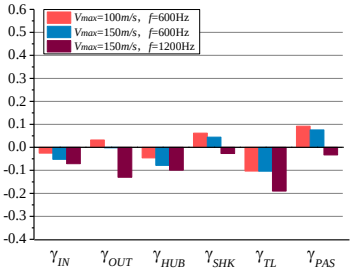

(a) 0T

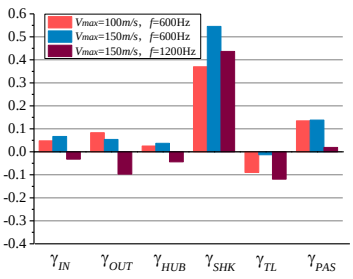

(b) 0.25T

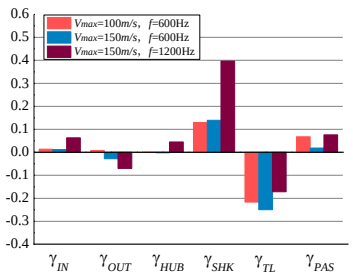

(c) 0.5T

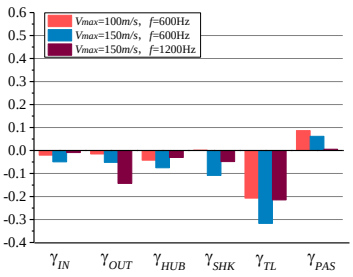

(d) 0.75T

Fig.17. Loss source change under synthetic jet excitation near the stall point (L=25%Ca).

separated under the action of the reverse pressure gradient. The combined effect of the two factors is the main reason for the stall of the transonic compressor.

(2) The excitation position of synthetic jet is the main factor affecting the stability margin of the transonic compressor. Under three sets of excitation parameters studied in this paper, when excited at 0%Ca, the performance of the compressor deteriorates overall. When excited at 25%Ca, the flow margin of the compressor is significantly expanded. When excited at the other three positions, the flow margin of the compressor does not change much. This indicates that 25%Ca is the best excitation

position for the endwall synthetic jet.

(3) The flow field analysis shows that when 25%Ca is excited, the mechanism by which the flow margin of the compressor can be expanded is that the synthetic jet is located above the blockage area of the compressor. When the synthetic jet is in the injection phase, the jet will partially blow off the low speed airflow at the tip of the blade. When the synthetic jet is in the suction stage, the suction will suck out the low speed airflow at the tip of the blade. This alternating effect of injection and suction weakens the tip leakage vortex and enhances the flow capacity of the compressor tip. At the same time, the calculation results in this paper show that the suction effect of the synthetic jet is more effective than the injection effect for improving the compressor margin.

(4) The excitation frequency and jet peak velocity of synthetic jet are the main factors affecting the aerodynamic performance of the compressor, but the jet frequency has a greater impact. The calculation results in this paper show that the flow margin, total pressure ratio and efficiency of the compressor change little after increasing the peak jet velocity. After continuing to increase the excitation frequency of the synthetic jet, the compressor has further improved the total pressure ratio and efficiency on the basis of expanding the flow margin. This shows that there may be a threshold for the jet frequency. Only when the jet frequency is greater than this threshold, the overall aerodynamic performance of the compressor can be improved In the next step, we will conduct experimental research on endwall synthetic jet excitation of axial compressor.

ACKNOWLEDGEMENTS

The authors would like to thank the support of National Science and Technology Major Project (No. 2017-II-0005-0018).

REFERENCES

Amitay, M. and A. Glezer (2002). Role of actuation frequency in controlled flow reattachment over a stalled airfoil. *AIAA Journal* 40(2), 209-216.

Bae, J. W., K. S. Breuer and C. S. Tan (2005). Active Control of Tip Clearance Flow in Axial Compressors. *Journal of Turbomachinery* 127(2), 352-362.

Benini, E., R. Biollo and R. Ponza (2011). Efficiency enhancement in transonic compressor rotor blades using synthetic jets: a numerical investigation. *Applied Energy* 88, 953-962.

Biela, C., Martin, W. Müller, H. P. Schiffer and C. Zscherp (2008). Unsteady Pressure Measurement in a Single Stage Axial Transonic Compressor Near the Stability Limit. *ASME Turbo Expo 2008*. American Society of Mechanical Engineers.

Chen, H., S. S. Koley, Y. Li and J. Katz (2019). Systematic Experimental Evaluations Aimed at Optimizing the Geometry of Axial Casing Groove in a Compressor. *ASME Turbo Expo 2019*: Turbomachinery Technical Conference and Exposition.

Culley, D. E., M. M. Bright, P. S. Prahst and A. J. Strazisar (2004). Active flow separation control of a stator vane using surface injection in a multistage compressor experiment. *Journal of Turbomachinery* 126(1), 24-34.

Giorgi, M. G. D. (2012). Active Flow Control Techniques on a Stator Compressor Cascade: A Comparison Between Synthetic Jet and Plasma Actuators. *ASME Turbo Expo 2012*: Turbomachinery Technical Conference and Exposition.

Li, X., W. Chu and Y. Wu (2014). Numerical investigation of inlet boundary layer skew in axial-flow compressor cascade and the corresponding non-axisymmetric end wall profiling. *Proceedings of the Institution of Mechanical Engineers, Part A: Journal of Power and Energy* 228(6), 638-656.

Li, X.，W. Chu, Y. Wu, H. Zhang and S. Spence (2016). Effective end wall profiling rules for a highly loaded compressor cascade. *Proceedings of the Institution of Mechanical Engineers, Part A: Journal of Power and Energy* 230(6), 535-553.

Ma, S., W. Chu, H. Zhang, X. Li and Kuang H. (2018). Effects of modifed micro-vortex generators on aerodynamic performance in a high-load compressor cascade. *Proceedings of the Institution of Mechanical Engineers Part A Journal of Power and Energy* 233(3), 309-323.

Ma, S., W. Chu, H. Zhang, X. Li and H. Kuang (2019). A combined application of micro-vortex generator and boundary layer suction in a high-load compressor cascade. *Chinese Journal of Aeronautics* 32(05),1171-1183.

Matejka, M., L. Popelka, P. Safarik and J. Nozicka (2008). Influence of Active Methods of Flow Control on Compressor Blade Cascade Flow. *ASME Turbo Expo 2008*: Turbomachinery Technical Conference and Exposition.

Qin, Y., Y. Song, F. Chen, R. Wang and H. Liu (2017). Active flow control by means of endwall synthetic jet on a high-speed compressor stator cascade. *Proceedings of the Institution of Mechanical Engineers, Part A: Journal of Power and Energy* 232(6), 641-659.

Reid, L. and R. Moore (1978). Design and overall performance of four highly-loaded, high speed inlet stages for an advanced high pressure ratio core compressor. *NASA Technical Paper*, TP-1337.

Saito, S., M. Furukawa, K. Yamada, K. Watanabe and N. Niwa (2019). Mechanisms and

Quantitative Evaluation of Flow Loss Generation in a Multi-Stage Transonic Axial Compressor. *ASME Turbo Expo 2019: Turbomachinery Technical Conference and Exposition.*

Smith, B. L. and A. Glezer (1998). The formation and evolution of synthetic jets. *Physics of Fluids* 10(9), 2281-2297.

Van Zante, D. E., A. J. Strazisar, J. R. Wood, M. D. Hathaway and T. H. Okiishi (2000). Recommendations for achieving accurate numerical simulation of tip clearance flows in transonic compressor rotors. *Journal of Turbomachinery* 122(4), 733-742.

Xu, H., B. Liu, L. Cai, X. Zhou, S. Wang and Z. Wang (2018). Influence of Oscillating Boundary Layer Suction on Aerodynamic Performance in Highly-Loaded Compressor Cascades. *ASME Turbo Expo 2018: Turbomachinery Technical Conference and Exposition.*

Yamada, K., K. Funazaki and H. Sasaki (2008). Numerical investigation of relation between unsteady behavior of tip leakage vortex and rotating disturbance in a transonic axial compressor rotor. *ASME Turbo Expo 2008: Turbomachinery Technical Conference and Exposition.*

Zander, V., M. Hecklau, W. Nitsche, A. Huppertz and M. Swoboda (2011). Active flow control by means of synthetic jets on a highly loaded compressor cascade. *Proceedings of the Institution of Mechanical Engineers, Part A: Journal of Power and Energy* 225(7), 897-906.

Zhang, H., Y. Wu, X. Yu, Y. Li and B. Liu (2019). Experimental Investigation on the Plasma Flow Control of Axial Compressor Rotating Stall. *ASME Turbo Expo 2019: Turbomachinery Technical Conference and Exposition.*

Zheng, X., A. Hou, Q. Li, S. Zhou and Y. Lu(2006). Flow control of annular compressor cascade by synthetic jets. *ASME Turbo Expo 2006: Turbomachinery Technical Conference and Exposition.*